LINEAR MODELING OF LOW-FREQUENCY DYNAMICS IN SEPARATED TURBULENT FLOW OVER A SMOOTH BUMP

Roman Klopsch
Department of Aeronautics
Imperial College London
roman.klopsch24@imperial.ac.uk

Lukas M. Fuchs
Flow Instabilities and Dynamics
Technische Universität Berlin

Georgios Rigas,
Department of Aeronautics
Imperial College London

Kilian Oberleithner
Flow Instabilities and Dynamics
Technische Universität Berlin

Jakob G. R. von Saldern
Flow Instabilities and Dynamics
Technische Universität Berlin

ABSTRACT

We present results from physics-based modeling of low-frequency dynamics in an incompressible separated turbulent flow over the *Boeing Gaussian Bump*. The Reynolds number is 2×10^6, based on the free-stream velocity and wind tunnel width, and the Mach number is 0.1. Particle Image Velocimetry (PIV) by Gray (2023) are used for validation of the modeling results. Linear Stability Analysis (LSA) is employed to model the flow dynamics, and identifies a modal mechanism at zero frequency that matches well with the observed low-frequency dynamics. In the literature, similar modal mechanisms are often attributed to centrifugal instabilities. Further analysis reveals that this modal mechanism relies on coherent energy production through the spatial gradient of the mean field-consistent eddy viscosity field. These results add to the discussion regarding the role of eddy viscosity in linear modeling of turbulent flows and highlight that the effects of a spatially-resolved eddy viscosity field are more nuanced than a spatially-varying dissipation model.

INTRODUCTION

For the study and modeling of coherent structures in turbulent separated flows, linearized mean field methods, including Linear Stability Analysis (LSA) and Resolvent Analysis (RA), have emerged as popular tools. These methods are based on a linearization of the Navier-Stokes equations around the temporal mean flow, which includes a closure term representing the nonlinear energy transfer. This closure problem is frequently tackled in analogy to the mean flow closure problem in the Reynolds-averaged Navier-Stokes (RANS) equations, through introduction of a turbulent (eddy) viscosity model. For the choice of eddy viscosity, the mean field-consistent value, available from data assimilation, has become a popular choice in recent years (Rukes *et al.*, 2016; Tammisola & Juniper, 2016; Symon *et al.*, 2023; Saldern *et al.*, 2024). However, the introduction of such a spatially-varying viscosity-like variable has the potential of modifying flow stability in unexpected ways (Govindarajan & Sahu, 2014). For turbulent mean flow analyses, these implications are rarely discussed.

In this paper, we discuss results from linear modeling of low-frequency dynamics in a separated flow over the *Boeing*

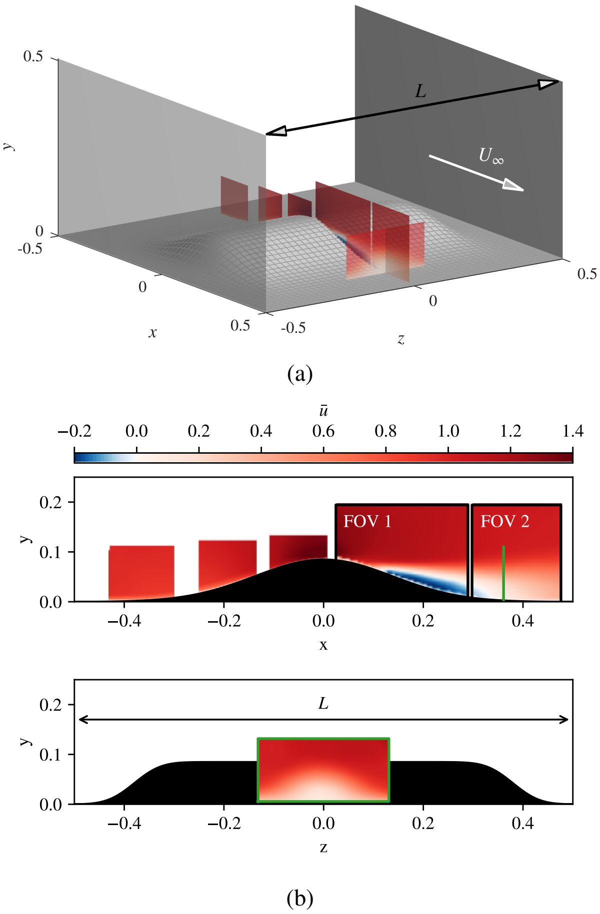

Figure 1: Geometry of the bump and $\bar{u}$ from PIV measurements. Reproduced from Klopsch *et al.* (2025*a*).

Gaussian Bump (Williams *et al.*, 2020; Gray *et al.*, 2021; Gray, 2023; Manohar *et al.*, 2026; Gray *et al.*, 2026). The flow is fully turbulent with a Reynolds number of $Re = 2 \times 10^6$, based on the free-stream velocity and wind tunnel width. The geometry of the bump including PIV mean fields from Gray (2023) is shown in Figure 1. An overview of the mean flow topology is provided in Gray *et al.* (2026). In the present study, we employ SPOD on the PIV snapshots to identify coherent structures, which are then modeled using LSA. The role of the mean field-consistent eddy viscosity field, used in constructing the linear operator, is subsequently discussed. This paper thereby extends on our previous studies on this flow: The data assimilation procedure used to obtain the mean flow for the linear analysis, including an eddy viscosity field, is detailed in Klopsch *et al.* (2025*b*). An extensive characterization of the flow dynamics in both cases, including linear modeling results are reported in Klopsch *et al.* (2025*a*).

METHODS

We employ both data-driven and physics based approaches to investigate coherent structures in the flow. On the data-driven side, we employ SPOD to the PIV snapshots. On the physics-based side, we employ global linear stability analysis. The linear analysis is then validated by comparison with the data-driven results.

Spectral Proper Orthogonal Decomposition

SPOD is applied to identify coherent structures in the turbulent broadband dynamics of the flow (Lumley, 1970; Towne *et al.*, 2018). Starting from a temporally and spatially resolved signal, in this case the PIV snapshot data, the cross-spectral density is estimated and the SPOD modes are given by its eigenvectors. The corresponding eigenvalue represents the spectral energy of the mode. If large parts of the spectral energy at a given frequency are contained in a small subset of the SPOD modes, the dynamics are considered *low-rank* and the dominant modes are considered *coherent structures* in the flow.

Global Linear Stability Analysis

We consider the Navier–Stokes equations with Reynolds decomposition $u = \bar{u} + u'$, where $\bar{u}$ denotes the time-averaged velocity field and u' the remaining fluctuating share. For the latter a modal ansatz of the form

$$u' = \hat{u} e^{\mathrm{i}\beta z - \mathrm{i}\omega t} + \text{c.c.}, \tag{1}$$

is assumed, where $\beta = 2\pi n$ and ω are the spanwise- and temporal wavenumber, and z and t the respective coordinates. The spanwise-harmonic ansatz allows the three-dimensional problem to be solved on a two-dimensional mesh. Introducing this ansatz in the linearized Navier–Stokes equations yields

$$-\mathrm{i}\omega\hat{\mathbf{u}} + (\bar{\mathbf{u}}\cdot\nabla)\hat{\mathbf{u}} + (\hat{\mathbf{u}}\cdot\nabla)\bar{\mathbf{u}} + \nabla\hat{p} - \nabla\cdot\left[(\frac{1}{Re} + \nu_t)\hat{\mathbf{S}}\right] = \hat{\mathbf{f}}, \tag{2}$$

where an eddy viscosity model (Boussinesq approximation) is introduced to close the equations. The model relates the deviatoric share of the coherent component of Reynolds stresses, $\widehat{u'u'}$, that represent the fluctuating Reynolds stresses in frequency space, to the coherent strain rate tensor $\hat{\mathbf{S}} = (\nabla + \nabla^\top)\hat{\mathbf{u}}$. The spherical part, representing isotropic normal stress, is absorbed into the pressure term. The deviation between the modeled and true coherent stresses is represented by the forcing vector $\hat{\mathbf{f}}$. This *ad hoc* model is commonly applied to the linearized Navier–Stokes equations and is important, as it introduces a turbulent dissipation term that is otherwise absent (Symon *et al.*, 2023; Saldern *et al.*, 2024).

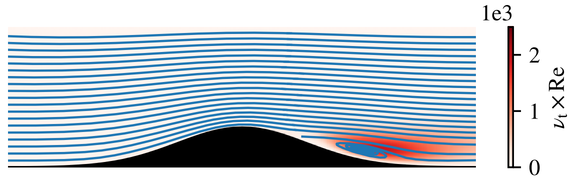

Figure 2: Data-assimilated mean flow used in the approximation of the linear operator, with the eddy viscosity field shown as background contours and mean streamlines overlaid in blue. Reproduced from Klopsch *et al.* (2025*a*).

The linearized continuity condition reads $\nabla\cdot\hat{\mathbf{u}} = 0$. Equation 2 and the continuity condition are cast into the linearized Navier–Stokes operator $\mathscr{L}$, allowing the system to be written as

$$-i\omega\hat{\mathbf{q}} = \mathscr{L}\hat{\mathbf{q}} + \hat{\mathbf{f}} \tag{3}$$

where $\hat{\mathbf{q}} = [\hat{\mathbf{u}}, \hat{q}]^\top$ is the state vector. Assuming ($\hat{\mathbf{f}} = \mathbf{0}$), Eq. 3 simplifies to an eigenvalue problem. The real and imaginary parts of the complex eigenvalue ω correspond to the frequency and growth rate of the mode, respectively, and the mode shape is given by the corresponding eigenvector.

The LSA computations are performed using *FELiCS*[1] (Kaiser *et al.*, 2023), an open-source linear flow solver developed at TU Berlin.

DATABASE

We work with the experimental database from the Smooth Body Separation Experiment[2] by Gray (2023), which includes various measurements of the flow over the *Boeing Gaussian Bump* at different Reynolds numbers. We consider the flow condition with Reynolds number $Re = 2\times10^6$, based on the free-stream velocity (34 m/s) and wind tunnel width (0.91 m). The corresponding Mach number is $M = 0.1$. At this Reynolds number, the flow is fully separated and a turbulent separation bubble is formed at the downstream face of the bump. PIV mean fields for the separated flow are shown in Figure 1. Time series of the velocity fields are available in "FOV 1" and "FOV 2" (u, v), and in the spanwise window (u, v, w).

In (Klopsch *et al.*, 2025*a*), we also analyse the flow conditions $Re = 10^6$ and $Re = 4\times10^6$. While the mostly attached flow at $Re = 10^6$ displays different dynamics, the dynamics at $Re = 4\times10^6$ remain largely unchanged compared to the present case.

To construct the linear operator used in the LSA formulation, velocity mean fields and their gradients, as well as a corresponding eddy viscosity field are required (see Eq. 2). These are publicly available[3] from our previous study (Klopsch *et al.*, 2025*b*), where we assimilated the flow using a Physics-informed Neural Network with the experimental PIV mean field serving as training data and the RANS equations alongside continuity and a no-slip wall condition as physical

[1] https://felics.eu/
[2] Data available in the Turbulence Modeling Resource: https://tmbwg.github.io/turbmodels/Other_exp_Data/speedbump_sep_exp.html
[3] https://git.tu-berlin.de/pida-group

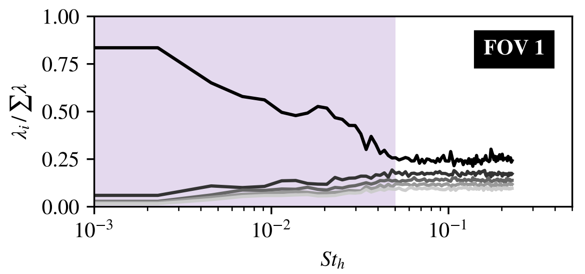

Figure 3: SPOD eigenvalue spectra from PIV time series data in "FOV 1" (Gray, 2023). Eigenvalues are normalised by the sum over all eigenvalues to highlight low-rank structure.

constraints. Pressure and mean field-consistent eddy viscosity fields are inferred in the process. Streamlines and eddy viscosity contours of the assimilated mean flows are shown in Figure 2. Further details on the data assimilation procedure, including a validation of the inferred pressure and eddy viscosity fields, can be found in the aforementioned study.

RESULTS

Detailed results from SPOD and linear modeling are available in our previous publication (Klopsch *et al.*, 2025*a*). A brief summary of the key aspects is provided in the first part of this section. In the second part, we focus on the role of the eddy viscosity field in the linear modeling approach, highlighting the production mechanism through the spatial gradient of the mean field-consistent eddy viscosity field.

Summary of Previous Results

A normalised SPOD eigenvalue spectrum computed for the PIV interrogation window "FOV 1" (see Figure 1) is shown in Figure 3. Here, $St_h = fh/U_\infty$ is the Strouhal number based on the bump height h and freestream velocity U_∞. We consider $St_h < 0.05$ as the low-frequency regime, as indicated by the purple-shaded area in the figure. For the lowest resolvable frequency (1 Hz, corresponding to $St_h = 2.3\times10^{-3}$), the leading mode accounts for around 80 % of the power spectral density. This demonstrates that the bump flow at this Reynolds number exhibits strong low-rank dynamics.

The pronounced low-frequency dynamics can be explained by a branch of global eigenvalues with distinctly elevated growth rate. The corresponding LSA spectrum is shown in Figure 4. Here, the x-axis shows the spanwise wave number $n = \beta/(2\pi)$, the y-axis shows the growth rate with a Strouhal-like scaling, and the color-axis shows the frequency expressed as Strouhal number. The critical branch consists of eigenvalues with (numerically) zero frequency and non-zero spanwise wave number. In the range of $2.5 < n < 12.5$, the modes are globally unstable.

The mode shape corresponding to the spanwise wave number with the largest growth rate, $n = 6.5$ (black cross in Figure 4), is shown in Figure 5a. The leading SPOD mode for the zero frequency bin is shown in Figure 5b, for comparison. Evidently, the mode shapes are similar. This observation leads us to consider the distinct global eigenvalue branch as a meaningful modeling result. This result is in line with previous observations in the literature on laminar and turbulent separation bubbles that similarly identified the low frequency unsteadiness to be rooted in a global eigenmode: Barkley *et al.* (2002); Gallaire *et al.* (2007); Rodríguez *et al.* (2013); Cura *et al.* (2024); Sarras *et al.* (2024); Savarino *et al.* (2025); Fuchs *et al.* (2026), to name a few.

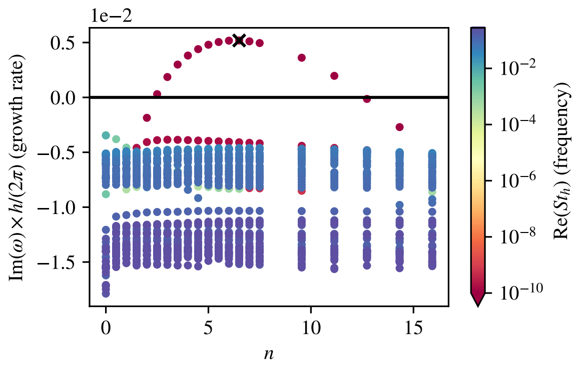

Figure 4: LSA eigenvalue spectrum. Reproduced from Klopsch *et al.* (2025*a*).

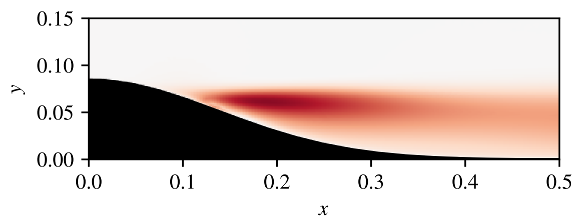

(a) LSA, $n = 6.5$

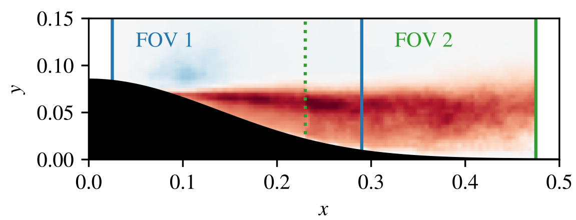

(b) SPOD

Figure 5: Zero frequency modes from LSA and SPOD. (a) LSA mode shape at $n = 6.5$; (b) leading SPOD mode. Adapted from Klopsch *et al.* (2025*a*).

Role of Eddy Viscosity in Flow Stability

The observation of globally unstable zero-frequency modes is somewhat unexpected in a linear mean-field analysis. Such a mode corresponds to a steady deformation of the flow field with growing amplitude, which is inconsistent with the converged mean field obtained from the measurements. The positive growth rates are thus likely rooted in the underlying modeling assumptions, namely the assumption of a homogeneous mean field in the spanwise direction and in the eddy viscosity closure used in the linearized equations.

It appears natural to assume that the positive growth rates result from a lack of dissipation, and that the growth rate could be suppressed by increasing ν_t to yield weakly-dampened modes, as done in (Fuchs *et al.*, 2026). Specifically, we define

$$\nu_t = \gamma\nu_{t,\mathrm{RANS}} \tag{4}$$

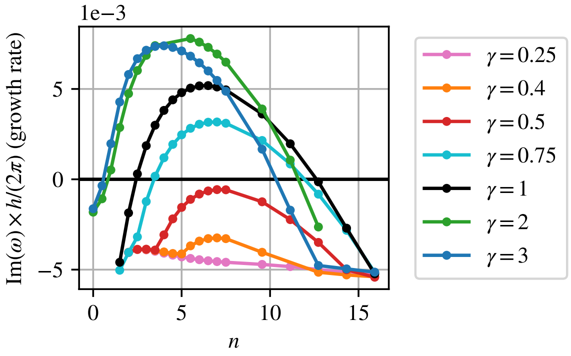

Figure 6: LSA critical eigenvalue branches as computed for different values of γ.

where $\nu_{t,\mathrm{RANS}}$ is the mean field-consistent value (in the baseline formulation $\gamma = 1$). The critical eigenvalue branches as computed for different values of γ are shown in Figure 6. Unexpectedly, increasing the eddy viscosity further destabilizes the eigenvalues, whereas decreasing it suppresses the growth rates, until the distinct modes vanish for $\gamma = 0.25$. This result is counter-intuitive, as the eddy viscosity is typically assumed to have a predominantly damping effect by introducing additional dissipation into the system.

In order to explain the destabilizing effect of the eddy viscosity, we study the respective term in the momentum equations. To this end, the eddy viscosity term is expanded using the product rule,

$$\nabla \cdot (\nu_t \hat{\mathbf{S}}) = \nu_t \nabla^2 \hat{\mathbf{u}} + (\nabla \nu_t) \cdot \hat{\mathbf{S}} \tag{5}$$

where the first term on the right hand side is analogous to the familiar (molecular) viscous term that includes viscous momentum transport and energy dissipation. The second, inhomogeneous term captures the effect of a spatially-varying viscosity. Under the common assumption of a spatially-uniform viscosity in aerodynamic flows, this term is typically neglected and the viscous term is solely written in terms of the velocity Laplacian.

Multiplying Eq. 5 with $\hat{\mathbf{u}}^*$ gives the respective contributions to the coherent energy balance (Symon *et al.*, 2023),

$$\hat{\mathbf{u}}^* \cdot \left[\nabla \cdot (\nu_t \hat{\mathbf{S}})\right] = \underbrace{\nu_t \hat{\mathbf{u}}^* \cdot (\nabla \cdot \hat{\mathbf{S}})}_{\text{homogeneous}} + \underbrace{\hat{\mathbf{u}}^* \cdot \left(\nabla \nu_t \cdot \hat{\mathbf{S}}\right)}_{\text{inhomogeneous}}, \tag{6}$$

where the homogeneous term on the right hand side can be further expanded by inverting the product rule,

$$\underbrace{\nu_t \hat{\mathbf{u}}^* \cdot (\nabla \cdot \hat{\mathbf{S}})}_{\text{homogeneous}} = \underbrace{\nu_t \nabla \cdot (\hat{\mathbf{u}}^* \cdot \hat{\mathbf{S}})}_{\text{transport}} - \underbrace{\nu_t (\nabla \hat{\mathbf{u}}^*) : \hat{\mathbf{S}}}_{\text{dissipation}}, \tag{7}$$

where the transport term is conservative and integrates to zero over a domain without boundary flux, and the dissipation term is an energy sink, provided $\nu_t > 0$. Therefore, the homogeneous term is always globally dissipative in the absence of boundary fluxes. The inhomogeneous term, however, is the product of two independent quantities, and the sign is not known *a priori*. The fields associated with both terms and the

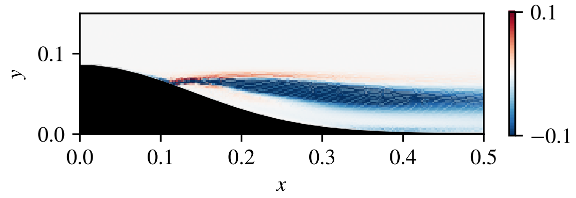

(a) homogeneous term: $\mathrm{Re}\left[\nu_t \hat{\mathbf{u}}^* \cdot (\nabla \cdot \hat{\mathbf{S}})\right]$

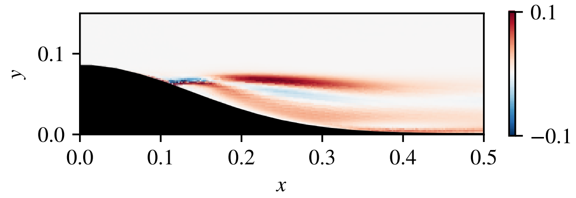

(b) inhomogeneous term: $\mathrm{Re}\left[\hat{\mathbf{u}}^* \cdot \left(\nabla \nu_t \cdot \hat{\mathbf{S}}\right)\right]$

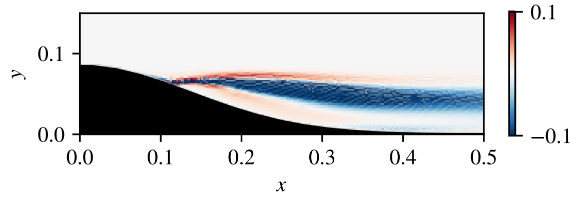

(c) total contribution: $\mathrm{Re}\left(\hat{\mathbf{u}}^* \cdot \left[\nabla \cdot (\nu_t \hat{\mathbf{S}})\right]\right)$

Figure 7: Eddy viscosity-related terms in the coherent energy balance. Normalized by respective maximum absolute value.

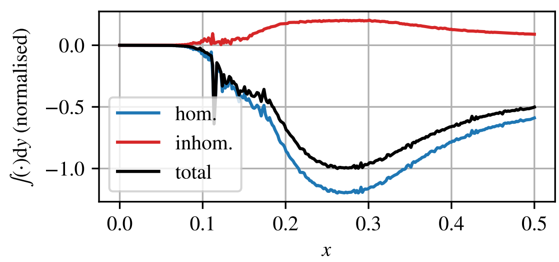

Figure 8: Vertically-integrated homogeneous (hom.) and inhomogeneous (inhom.) eddy viscosity terms in the coherent energy balance, and the sum of both terms.

total contribution are plotted in Figure 7. Evidently, the homogeneous term primarily dissipates coherent energy, whereas the inhomogeneous term acts mainly as a production term. This is further highlighted in Figure 8, where the terms are integrated over the vertical coordinate y. All curves are normalized by the maximum absolute value of the total contribution. Clearly, the overall direct effect of the eddy viscosity is primarily dissipative due to the dissipative contribution through the homogeneous term being significantly larger than the productive contribution through the inhomogeneous term. Nevertheless, the total contribution of the eddy viscosity to the coherent energy balance is locally positive in some regions of the flow (see Figure 7c), including the recirculation bubble.

In order to verify that the inhomogeneous contribution is

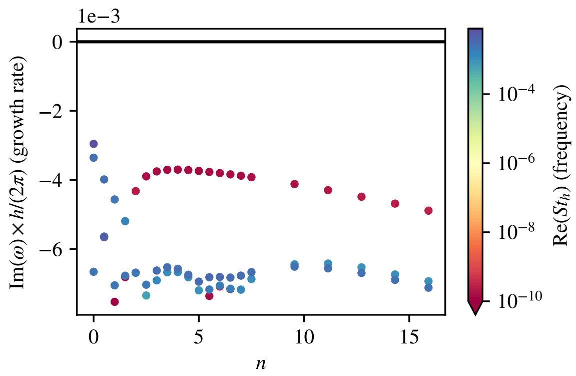

(a) Mean field-consistent, spatially-resolved ν_t with the inhomogeneous term neglected in the equations

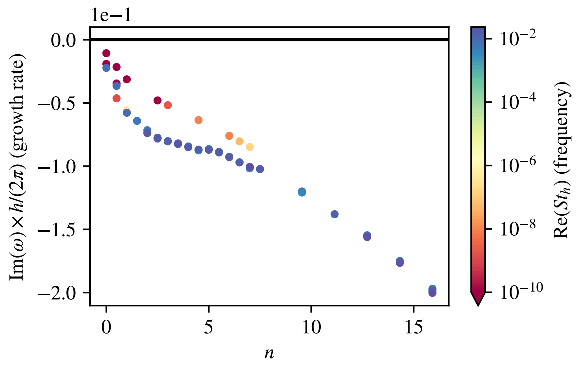

(b) Spatially-constant $\nu_t = 9.4 \times 10^{-4}$

Figure 9: LSA eigenvalue spectra with modified eddy viscosity models.

in fact responsible for destabilizing the eigenvalue branch at zero-frequency, we remove the term that includes the eddy viscosity gradient from the linearized equations in our stability solver, and repeat the LSA. For this analysis, the eddy viscosity is set to the mean field consistent field with $\gamma = 1$. The resulting eigenvalue spectrum is shown in Figure 9a (compare to Figure 4). For comparison, we also perform the LSA with a constant $\nu_t = 9.4 \times 10^{-4}$, which corresponds to the mean field-consistent value in the center of the bubble. The eigenvalue spectrum for this case is shown in Figure 9b. For both cases, the critical eigenvalue branch is not captured, and none of the identified mode shapes represent physically meaningful features (not shown). These results indicate that coherent energy production through the inhomogeneous term significantly impacts the linear stability predictions and, for the present case, is essential for modeling the mode shown in Figure 5a using LSA.

The observation of instabilities resulting from viscosity gradients is not new. For laminar flows with spatially-varying molecular viscosity (e.g. due to concentration or temperature gradients), such instabilities have been studied for decades, as summarized in the review by Govindarajan & Sahu (2014). For a linear mean flow analysis of a turbulent channel flow with eddy viscosity model, Symon *et al.* (2021) discuss energy production associated with eddy viscosity gradients and conclude that the model remains primarily dissipative. Based on the results shown in Figure 8, a similar conclusion could be drawn for the present case. This result of a primarily dissipative behavior also holds for the scaled eddy viscosities with factor γ, as the scaling affects the homogeneous and inhomogeneous contributions equally.

However, the present results demonstrate that the integral contribution to the energy budget is insufficient to conclude whether the terms stabilize or destabilize the system. Instead, the spatial distribution of the individual contributions is crucial, as local positive contributions to the energy budget may act as a forcing (in analogy to resolvent analysis), generating structures that are subsequently amplified through interaction with the mean flow gradients.

CONCLUSIONS

From the results presented in this study, several conclusions can be drawn regarding turbulence modeling in stability analyses of the separated turbulent flow over the *Boeing Gaussian Bump*. Introducing a spatially resolved eddy viscosity, such as the mean-field-consistent value, can give rise to additional eigenmodes that rely on coherent energy production through gradients of the eddy viscosity field and are not observed for a spatially constant value. This mechanism is also responsible for the somewhat counter-intuitive observation, that artificially increasing the eddy viscosity further destabilizes the eigenvalue branch, whereas stabilization can be achieved by reducing its value.

For the present case, the resulting eigenvalue branch shows close agreement with the coherent structures identified in the PIV data. In particular, the zero-frequency eigenmode ($St_h = 0$) is consistent with the corresponding SPOD mode and accounts for a significant fraction of the low-frequency power spectral density in the velocity snapshots. These findings contribute to the ongoing discussion on closure modeling in the linearized equations and highlight the need for further research to better understand potentially unexpected effects associated with spatially resolved eddy viscosity models, including mean-field-consistent formulations.

REFERENCES

Barkley, Dwight, Gomes, M. Gabriela M. & Henderson, Ronald D. 2002 Three-dimensional instability in flow over a backward-facing step. *Journal of Fluid Mechanics* **473**, 167–190.

Cura, C., Hanifi, A., Cavalieri, A.V.G. & Weiss, J. 2024 On the low-frequency dynamics of turbulent separation bubbles. *Journal of Fluid Mechanics* **991**, A11.

Fuchs, Lukas M., Steinfurth, Ben, Saldern, Jakob G. R. von, Weiss, Julien & Oberleithner, Kilian 2026 Standing-wave dynamics in low-frequency breathing of a turbulent separation bubble. *Journal of Fluid Mechanics* **1030**, A34.

Gallaire, François, Marquillie, Matthieu & Ehrenstein, Uwe 2007 Three-dimensional transverse instabilities in detached boundary layers. *Journal of Fluid Mechanics* **571**, 221–233.

Govindarajan, Rama & Sahu, Kirti Chandra 2014 Instabilities in Viscosity-Stratified Flow. *Annual Review of Fluid Mechanics* **46** (Volume 46, 2014), 331–353.

Gray, Patrick 2023 An Experimental Investigation of Smooth-Body Separation over a Tapered Gaussian Bump. PhD thesis, University of Notre Dame.

Gray, Patrick, Gluzman, Igal, Thomas, Flint & Corke, Thomas C. 2026 Smooth-body flow separation over a tapered Gaussian bump – flow field topography and topology. *Journal of Fluid Mechanics* **1032**, A54.

Gray, Patrick D., Gluzman, Igal, Thomas, Flint, Corke, Thomas, Lakebrink, Matthew & Mejia, Kevin 2021 A New Validation Experiment for Smooth-Body Separation.

In *AIAA AVIATION 2021 FORUM*. VIRTUAL EVENT: American Institute of Aeronautics and Astronautics.

Kaiser, Thomas L., Demange, Simon, Müller, Jens S., Knechtel, Sophie & Oberleithner, Kilian 2023 FELiCS: A Versatile Linearized Solver Addressing Dynamics in Multi-Physics Flows. In *AIAA AVIATION 2023 Forum*. San Diego, CA and Online: American Institute of Aeronautics and Astronautics.

Klopsch, Roman, Fuchs, Lukas M., Rigas, Georgios, Oberleithner, Kilian & von Saldern, Jakob G. R. 2025*a* Spectral analysis of attached and separated turbulent flows over a Gaussian-shaped bump.

Klopsch, Roman, Fuchs, Lukas M., Rigas, Georgios, Oberleithner, Kilian & Von Saldern, Jakob G. 2025*b* Enabling Resolvent Analysis Through Assimilation of Experimental Mean Flows with Physics-Informed Neural Networks: A Case Study on the Boeing Gaussian Bump. In *AIAA AVIATION FORUM AND ASCEND 2025*. Las Vegas, Nevada: American Institute of Aeronautics and Astronautics.

Lumley, John L. 1970 *Stochastik Tools in Turbulence*. *Applied Mathematics and Mechanics* 12. New York: Academic Press.

Manohar, Kevin H., Annamalai, Hariprasad, Williams, Owen, Morton, Chris & Martinuzzi, Robert J. 2026 Unsteadiness in turbulent separated flow over a three-dimensional Gaussian bump. ArXiv:2603.05765 [physics].

Rodríguez, Daniel, Gennaro, Elmer M. & Juniper, Matthew P. 2013 The two classes of primary modal instability in laminar separation bubbles. *Journal of Fluid Mechanics* **734**, R4.

Rukes, Lothar, Paschereit, Christian Oliver & Oberleithner, Kilian 2016 An assessment of turbulence models for linear hydrodynamic stability analysis of strongly swirling jets. *European Journal of Mechanics - B/Fluids* **59**, 205–218.

Saldern, Jakob G. R. von, Schmidt, Oliver T., Jordan, Peter & Oberleithner, Kilian 2024 On the role of eddy viscosity in resolvent analysis of turbulent jets. *Journal of Fluid Mechanics* **1000**, A51.

Sarras, K., Tayeh, C., Mons, V. & Marquet, O. 2024 Linear stability analysis of turbulent mean flows based on a data-consistent Reynolds-averaged Navier–Stokes model: prediction of three-dimensional stall cells around an airfoil. *Journal of Fluid Mechanics* **1001**, A41.

Savarino, Flavio, Sipp, Denis & Rigas, Georgios 2025 Optimal transitional mechanisms of incompressible separated shear layers subject to external disturbances. *Journal of Fluid Mechanics* **1016**, A43.

Symon, Sean, Illingworth, Simon J. & Marusic, Ivan 2021 Energy transfer in turbulent channel flows and implications for resolvent modelling. *Journal of Fluid Mechanics* **911**, A3.

Symon, Sean, Madhusudanan, Anagha, Illingworth, Simon J. & Marusic, Ivan 2023 Use of eddy viscosity in resolvent analysis of turbulent channel flow. *Physical Review Fluids* **8** (6), 064601.

Tammisola, O. & Juniper, M. P. 2016 Coherent structures in a swirl injector at Re = 4800 by nonlinear simulations and linear global modes. *Journal of Fluid Mechanics* **792**, 620–657.

Towne, Aaron, Schmidt, Oliver T. & Colonius, Tim 2018 Spectral proper orthogonal decomposition and its relationship to dynamic mode decomposition and resolvent analysis. *Journal of Fluid Mechanics* **847**, 821–867.

Williams, Owen, Samuell, Madeline, Sarwas, E. Sage, Robbins, Matthew & Ferrante, Antonino 2020 Experimental Study of a CFD Validation Test Case for Turbulent Separated Flows. In *AIAA Scitech 2020 Forum*. Orlando, FL: American Institute of Aeronautics and Astronautics.